OKU Fen Bilimleri Enstitüsü Dergisi
7(3): 1358-1373, 2024

OKU Journal of The Institute of Science and Technology, 7(3): 1358-1373, 2024

Osmaniye Korkut Ata Üniversitesi Fen Bilimleri Enstitüsü Dergisi

Osmaniye Korkut Ata University Journal of The Institute of Science and Technology

The Impact of Using Dimpled Surfaces on Ahmed Body on The Flow Characteristics

Veli Kemal AYDIN[1], Mustafa Atakan AKAR[2*], Oğuz BAŞ[3], Umut KUMLU[4]

[1,2,4]Çukurova University, Department of Automotive Engineering, 01330, Adana, Türkiye
[1]Kırpart Otomotiv Sanayi A. Ş , 16800 , Bursa, Türkiye
[3]Amasya University, Faculty of Technology, Department of Mechanical Engineering, Amasya, Türkiye

[1]https://orcid.org/0009-0000-9066-0974
[2]https://orcid.org/0000-0002-0192-0605
[3]https://orcid.org/0000-0003-2301-2306
[4]https://orcid.org/0000-0001-7624-6240
*Corresponding author: aakar@cu.edu.tr

Research Article

Article History:
Received: 08.11.2023
Accepted: 28.02.2024
Published online:25.06.2024

Keywords:
Drag coefficient
Lift coefficient
Aerodynamics
Computational fluid dynamics (CFD)
Ahmed body

ABSTRACT

Vehicle aerodynamics which directly affects fuel consumption values in vehicles has great importance in terms of vehicle stability, acceleration ability, vehicle noise, and environmental pollution. Ahmed car model is one of the most important generic models, so this popular car model is widely used in the literature on fluid mechanics and vehicle aerodynamics studies. This study investigated the effect of a passive drag reduction technique which is known as dimple surface, on the Ahmed car model with a 35° slant angle. The flow control methods were applied numerically also these methods were compared with similar works. Analysis made in this study was conducted with 2.4 million cell numbers and the maximum drag reduction is 3.5 % with optimum dimple surfaces. Moreover, the applicability and manufacturability factors were also evaluated in terms of implementing the dimpling modification to today's current road vehicles.

Ahmed Cisminde Çukurlu Yüzeyler Kullanmanın Akış Karakteristiklerine Etkisi

Araştırma Makalesi

Makale Tarihçesi:
Geliş tarihi: 08.11.2023
Kabul tarihi: 28.02.2024
Online Yayınlanma: 25.06.2024

Anahtar Kelimeler:
Sürükleme kuvveti katsayısı
Kaldırma kuvveti katsayısı
Araç aerodinamiği
Hesaplamalı akışkanlar dinamiği (CFD)
Ahmed cismi

ÖZ

Araç yakıt tüketim değerlerini doğrudan etkileyen araç aerodinamiği aynı zamanda araç stabilitesi, hızlanma yeteneği, araç sesi ve çevre kirliliği açısından büyük öneme sahiptir. Ahmed cismi jenerik araç modeli akışkanlar mekaniği ve araç aerodinamiği konusunda yapılan çalışmalarda çok fazla kullanılmaktadır. Akış kontrol yöntemlerinin numerik olarak araştırıldığı bu çalışmada sonuçlar deneysel veriler referans alınarak doğrulanmıştır. Bu çalışmada çukur yüzey olarak bilinen pasif sürükleme azaltma tekniğinin 35° eğik açılı Ahmed araba modeli üzerindeki etkisi araştırılmıştır. Analizler 2.4 milyon mesh sayısı ile çözümlenmiş olup, çukurcuklu yüzeylerin kullanılması ile en iyi modelde sürükleme kuvveti katsayısında %3,5 azalma elde edilmiştir. Aynı zamanda bu çalışmanın aerodinamik açısından anlamlı olması için uygulanan bu çukur yüzeylerin günümüz araçlarına uygulanabilirliği ve üretilebilirlik faktörü de değerlendirilmiştir.

To Cite: Aydın VK., Akar MA., Baş O., Kumlu U. The Impact of Using Dimpled Surfaces on Ahmed Body on The Flow Characteristics. Osmaniye Korkut Ata Üniversitesi Fen Bilimleri Enstitüsü Dergisi 2024; 7(3): 1358-1373.

1. Introduction

Nowadays continuously increasing fuel prices and climate change effect have caused fuel efficiency to become an important issue in the vehicle production industry. Also, the significant rise in the usage of energy resources with population growth and fuel consumption is becoming more critical.

The main objectives are the reduction of fuel consumption values which depend on three essential parameters: engine performance, car weight, and coefficient of drag to enhance fuel economy (Abd-Alla, 2002) (Peter et al., 2010) (Muyl et al., 2004). The drag coefficient of a vehicle plays an important role in the total fuel consumption value. For a sedan car at 100 km/h approximately 20 % of total fuel consumption and for a heavy car 50 % of total fuel consumption is used to overcome drag forces (M.Brady et al., 1999). Therefore, improving vehicle design and overcoming design limitations to reduce the coefficient of drag is an important step all over the vehicle design process in the automotive industry (Howell et al., 2002).

Two types of drag forces exist in aerodynamics which are pressure and friction drag. The pressure drag occurs from the pressure difference between the front and rear of the body and it is related to the form of aerodynamic design and flow detachment. However, friction drag is caused by friction between the air and the body and it affects the viscosity of air which is directly related to the Reynolds number and surface area of the body.

In aerodynamics studies, wind tunnel experiments are very successful to simulate real conditions and obtaining reliable results of the analysis. However, testing each optimization may lead to high costs and waste of time. However, with the developing technology and high-performance computers in Computational fluid dynamics (CFD) software has been an alternative for wind tunnel experiments.

In the Automotive industry, there are many reference car models, which are called generic ground models. Generic ground models are generally used in literature as a simulation model and each generic model has a specific characteristic aerodynamics depending on analysis conditions. These generic models are also named bluff bodies and these bodies have flow separation zones and characteristics of wake flow region (Kamal et al., 2021). This flow separation causes a lower pressure in the rear wake zone and all the optimization studies aim to reduce the big pressure difference between relatively higher-pressure zone and lower pressure zone.

Ahmed Body generic model is one of the important simulation tools in automotive aerodynamics literature. The model is easy to create and analyze because of its simple geometric shape compared to commercial vehicles (Howell et al., 2002). Even if it has a simple shape, it can create complex flow characteristics like commercial vehicles. A demonstration of full-scale Ahmed Body dimensions and slant angle variations can be seen in Figure 1.

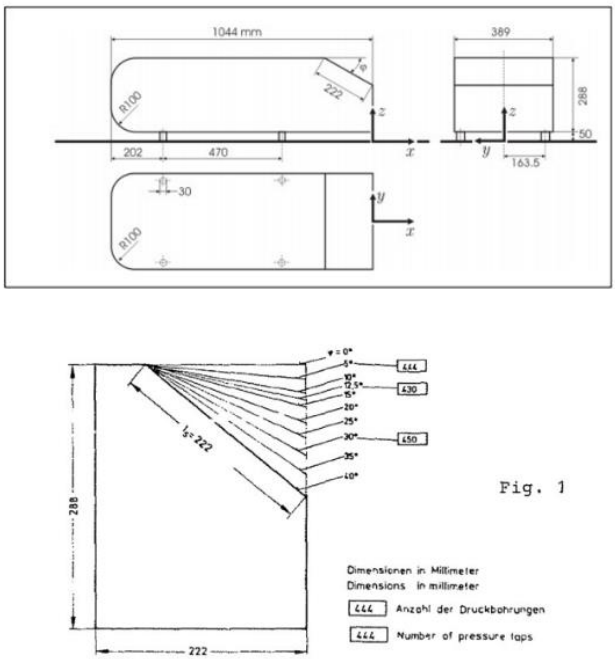

Figure 1. Schematic of Ahmed Body Dimensions and Slant Angle Variations (Ahmed et al., 1984)

Three major components of Ahmed body are the front cylindrical surface, longitudinal part, and angled rear window. The main flow separation occurs at the angled rear window area with the air coming from the top, bottom, and side areas. These separated and unformed shear layers after the end of the vehicle tend to each other because of a stagnation zone occurs. This zone created by layers is called the wake zone. The drag coefficient versus variation of the slant angle can be seen in Figure 2.

At the beginning of the slant angled area flow starts to separate and at the end of the slant area flow reforms to a separating bubble shape. To see the effect of slant angle on vehicle aerodynamics in the range of 0º to 40º angle values was studied by (Ahmed et al., 1984). According to this study, two critical angle values were detected which are 12.5º and 30º. Investigating the wake structure of the body has shown a significant increment detected between the values 12.5º and 30º (Lienhart et al., 2022). If the angle value is around 30 º, C-pillar vortices increase because of pressure drop on the slant area with the effect of separating the bubble. Over the 30 º slant angle the C-pillar becomes less strong because flow could not reattach to the slant angle surface compared to previous angle values. Therefore, the maximum drag coefficient value was at 30 º, and over these values decreased (Vino et al., 2005).

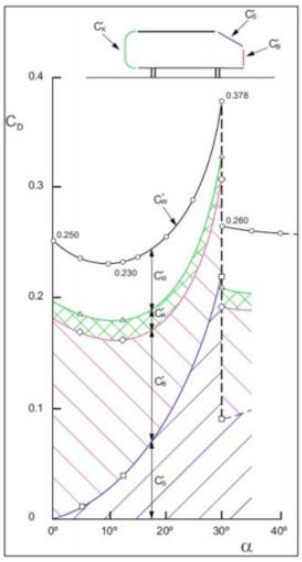

Figure 2. Ahmed body drag coefficient (Cd) variation with the change of slant angle (α) (Ahmed et al., 1984)

In this study, the slant angle value was not a variable parameter, and was selected as 35º. The significant characteristics flow of Ahmed body with flow separation and recirculation areas in the wake can be seen in Figure 3. As mentioned, the wider and greater wake region area is the main reason of the strong C-pillar vortices and high drag coefficient (Leroyer et al., 2011). There are some methods to eliminate the sudden pressure drop on the wake region and these methods are divided into active and passive methods depending on energy addition the control system (Altaf et al., 2014).

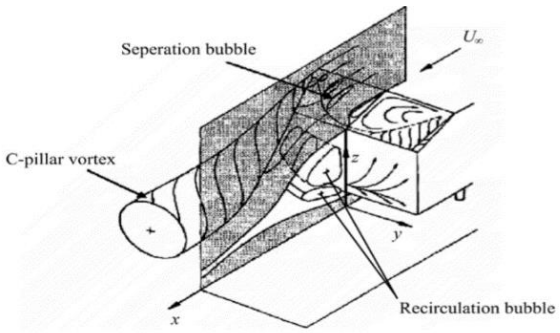

Figure 3. Averaged near wake structure of Ahmed model of α= 12.5-30 (Ahmed et al., 1984)

Active control methods need external energy synchronized with the vehicle's energy distribution system. These active methods work in harmony with more than one engineering system like electromagnetic, mechanic, electric, piezoelectric, and acoustic. Contrary to passive methods, active methods mostly use moveable wings, walls, vortex generators, covers, or grills to control flow depending on a vehicle's velocity. Of course, design, size, and weight parameters are very critical since they can negatively affect when joined in the vehicle system. It can be understood from all that, active drag reduction methods are more complicated and have higher costs so that it is difficult to perform and work on with them.

Generally, passive control methods include body modification or add on operations on the vehicle surface. They are divided into two categories and how it affects the flow. The first category includes

barriers directly mounted on the vehicle surface and the second category consists of barriers located in the upper or lower position of the vehicle.

The objective body used in this study was demonstrated by (Ahmed et al., 1984). Even though Ahmed body was simple and available for CFD analysis, each turbulence model was not capable of solving the rear wake turbulence zone. That could be the reason why some of the studies in the literature aimed to investigate the predicting capabilities of turbulence models for different conditions. For example, a study was made by (Krajnovic et al., 2004) implemented a Large-Eddy simulation model flow around the Ahmed body. Large-Eddy Simulation (LES) is a CFD method that solves large flow wakes using Navier Stokes equations directly. But LES was an effective medium scale of Reynolds number it was capable of the direct solution instead of to modeling. Moreover, LES necessitates high computational resources and time when simulating highly turbulent flow. In another study, (Kapadia et al., 2004) studied a different CFD modeling technique as Detached Eddy Simulation (DES) with a cell number of 1.74 million. 25° and 35° slant angle Ahmed body models were analyzed, and results showed a 5% approximate value was taken according to experimental results (Ahmed et al., 1984).

Despite the DES and LES techniques having had perfect predicting capabilities of flow, they could not be used in some studies due to the computer requirements and more solution time. However, Reynolds-averaged Navier Stokes (RANS) based turbulence models are good alternative methods and very common in the automotive industry. Ahmed body with 25° was modeled by (Jakirlic et al., 2001) with the Realizable k-ε model and 2.3 million cell numbers and it is stated that despite the RANS models not being very good to predict flow separation characteristics, the result of this study can be in acceptable accuracy.

To create smaller wake flaps or deflectors, splitter plates, boat tails, vortex generators, and non-smooth surfaces one of the passive drag reduction methods. Implementing a vortex generator on Ahmed body 25° slant angle on 20 m/s free stream velocity provides 11.7 % maximum drag reduction. Vortex generators are positioned on top of the Ahmed body surface at a determined distance to control flow and prevent early separation (Krajnovic et al., 2004). Analysis in this study has been done with Ansys CFD commercial software.

Non-smooth surfaces are a very effective technique for reducing drag coefficient and making proper flow separation rear surface of Ahmed body. Dimpled surfaces are good examples of non-smooth surfaces. Dimpled surfaces on a golf ball that provide longer distance travel if compared to a non-dimpled surface ball are inspired by engineers. Because of long distance travel, it provides lower turbulent air in flow separation areas with the aid of dimpled surfaces. In Figure 4 the wake characteristics of golf balls are compared with dimple surfaces and without dimples.

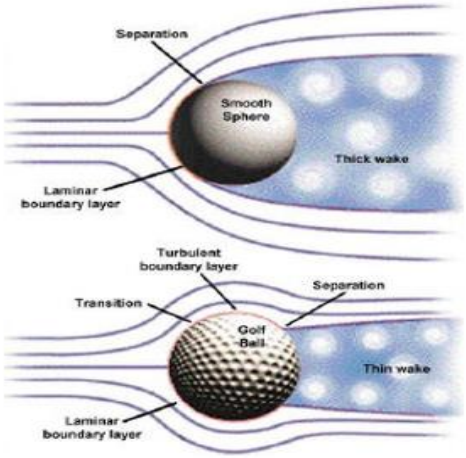

Figure 4. Dimpled surfaces on a golf ball (Chear et al., 2015)

From this point of view, in this study, Ahmed body with dimpled surfaces was investigated to compare flow and wake region characteristics. During CFD simulations, poly-hex core meshed CFD setups were solved with k-w SST turbulence model. The main objective of the study is to evaluate the drag coefficient and see the effect of variable design parameters of dimpled surfaces on vehicles. Furthermore, reducing the drag coefficient of an automobile improves the performance of the vehicle and fuel efficiency so the main purpose of the study was to reduce energy losses and inefficiencies by making aerodynamic improvements on the road vehicle model Ahmed body with an angle of 35°.

2. Material and Methods

2.1 Cad Model

As seen in Figure 1, the dimensions of the model; length L = 1044 mm; width W = 389 mm; height H = 288 mm; length of slant back E = 222 mm. Also, the diameter of the cylinders (stilts) is 30 mm and the height values of them are 50 mm from the origin. CATIA software was used to create 3D models of Ahmed body. In this study, dimples were used as a passive drag reduction technique on Ahmed body rear window area. Dimple characteristics have been defined by the surface roughness formula (Chear et al., 2015):

$$\boldsymbol{Dimple\ depth\ ratio} = \frac{\boldsymbol{k}}{\boldsymbol{d}} \tag{1}$$

k defines the dimple depth value and d defines the diameter value.

There are 15 different dimpled models used in simulations while they were configured with 3 different diameters. Also, each model has different depth values in its own group. It can be seen from Figure 5 and Table 1 that dimple surfaces were implemented with the same configurations on Ahmed body rear window are in all models. Additionally, to prevent a sharp surface between the rear window and the

dimples, 0.5 mm fillet radius was applied between the intersections of the dimples and the flat rear surface of the model.

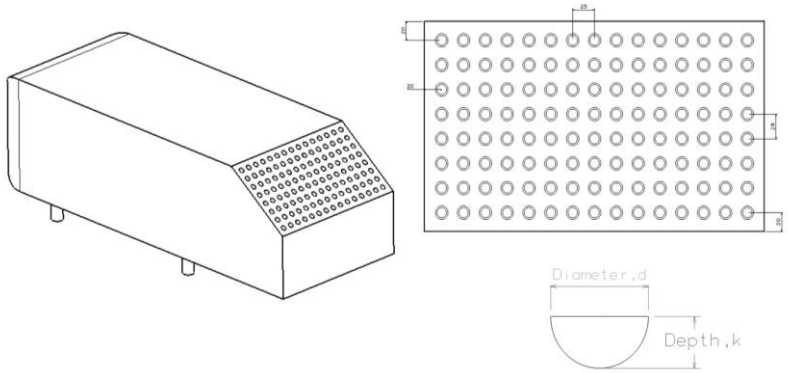

Figure 5. Ahmed body with dimple surfaces and dimensions in mm

Table 1. Diameter and depth values for each model

Model Number	10d1h	10d2h	10d3h	10d4h	10d5h	15d1h	15d2h	15d3h	15d4h	15d5h	20d1h	20d2h	20d3h	20d4h	20d5h
Dimple Diameter (mm)	10	10	10	10	10	15	15	15	15	15	20	20	20	20	20
Dimple Depth	1	2	3	4	5	1	2	3	4	5	1	2	3	4	5
Surface Roughness (ε)	0.1	0.2	0.3	0.4	0.5	0.06	0.13	0.2	0.26	0.33	0.05	0.1	0.15	0.2	0.25

2.2 Mesh generation and mesh independence

In CFD simulations, mesh resolution should be chosen rigorously. For example, in case of creating too fine or too coarse grid structure, it is possible to over-resolve or under-resolve the solution. Choosing a tiny mesh element size completely on the flow region causes high solution time and computational source requirement while low-resolution in mesh size may lead to sacrificing accuracy.

In this study, the flow region was separated into 3 different regions, the mesh resolution increased from the free-stream flow region to the vehicle body wall. To generate meshes for CFD simulations, the Watertight Geometry workflow tool in Ansys Fluent was used. The usage of this tool is so simple and simplifies mesh generation that it provides to complete all stages in one window. Also, thanks to the new poly-hexcore meshing algorithm, it is possible to improve mesh quality and reduce element quantity without compromising accuracy.

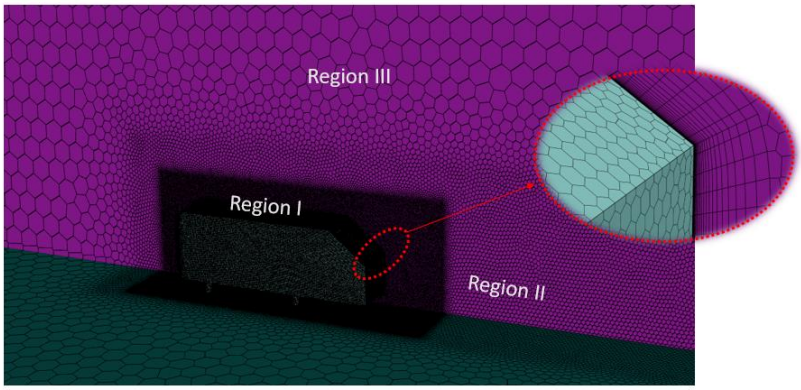

Figure 6. View of grid regions with 3 different mesh densities

As demonstrated in Figure 6, to make strategic mesh refinement, the flow domain was divided into 3 flow regions. The closest region to vehicle walls had the smallest mesh sizes to resolve flow characteristics around the vehicle. The y^+=1 strategy for first cell height was sustained as an essential requirement when solving viscous sublayer with k-ω SST to take advantage of this model. Also, 24 prism layers were used to increase the modelling of the capability of a fully turbulent boundary layer profile and the effect of the adverse gradient forces. Additionally, in numerical simulations mesh independence study was very vital to select an available and sensible number of mesh cells. In this study, as can be seen from Table 2, each region was analyzed with 3 different levels which were Mesh 1, Mesh 2, and Mesh 3. According to the results of the mesh independence tests represented in Figure 7, it was found that flow solutions were almost independent of grid size after the grid level of Mesh 2.

Table 2. Mesh sizing strategy

	Mesh 1	Mesh 2	Mesh 3
Element Size of region I (mm)	20	7.5	5
Element Size of region II (mm)	40	17.5	12.5
Element Size of region III (mm)	175	100	75
First prism layer height (mm)	0.04	0.04	0.04
Number of prism layer	24	24	24
Growth rate	1.2	1.2	1.2
Volume mesh type	Poly-hexcore	Poly-hexcore	Poly-hexcore
Total mesh count (x10^6)	1.1	2.4	5.5

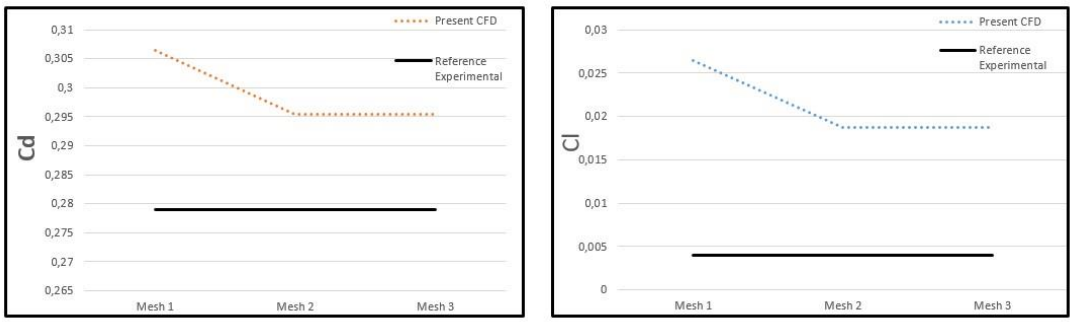

Figure 7. Mesh independence study

2.3 Turbulence Model

SST k-ω RANS model was adopted for numerical simulations in this study since it was advantageous in terms of computational cost compared with Detached Eddy Simulations (DES), Large Eddy Simulations (LES), and Unsteady Reynolds-Averaged Navier-Stokes (URANS). The main aim of k-ω Shear Stress Transport (SST) (Menter et al., 1992) was to utilize the aerodynamic modelling superiority of the model. SST k-ω model was used widely in aerodynamic studies so that it combined modelling capabilities of k-ω and k-Ɛ on near the walls and free shear layers far from surfaces.

2.4 Boundary conditions, solver settings, and post-processing

Air was set as fluid which was assumed constant properties and be incompressible. The air velocity was set to 40 m/s corresponding a Reynolds number of Re = $2{,}86\ x\ 10^6$ was based on length of the Ahmed body. The turbulence intensity value was selected at 0.5%. Also, the pressure outlet value was set to 0 Bar gauge pressure with 5 % turbulence intensity. These turbulent intensity values were selected to simulate the experimental results of (Meile et al., 2011) in this study. The experimental results of (Ahmed et al., 1984) at Re = $4.29\ x\ 10^6$ are included also to verify the result of this study. The 'Double Precision' setting was selected to increase the accuracy of the solution. Parallel processing options were chosen instead of serial and the number of processes were selected considering the hardware facilities of the solver computer.

The spatial discretization was selected 2nd order upwind for the momentum and pressure. Additionally, convergency criteria values were 10^{-5} for all residuals to attain high accuracy.

The boundary conditions and flow parameters used in the numerical solutions are shown in Table 3. As can be seen from Figure 8, the size of the flow domain was generated big enough to obtain fully developed flow before the body and resolve wake completely. A quasi-3D was used to reduce the number of elements and analyze time.

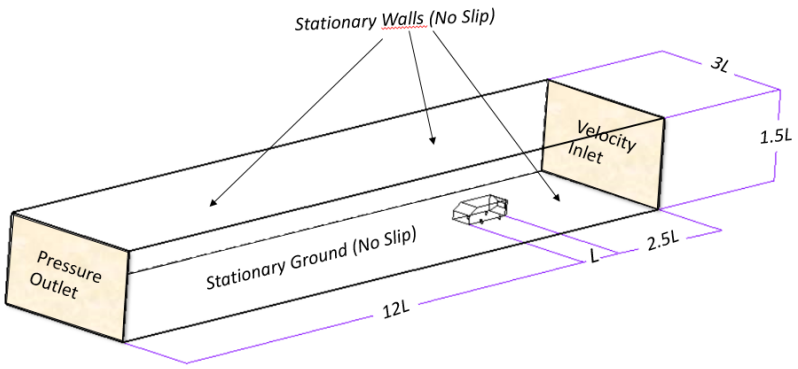

Figure 8. Dimensions and boundary conditions of the computational domain

Table 3. Boundary condition setup for numerical analysis

Boundary Condition Parameters	Boundary Condition Type	Quantity
Inlet	Velocity inlet	40 m/s
Outlet	Pressure outlet	1 atm
Walls (Ahmed body)	Stationary wall with no-slip condition	_
Walls (Enclosure)	Stationary wall with no-slip condition	_

The general CFD approach applied in this study can be seen in Figure 9.

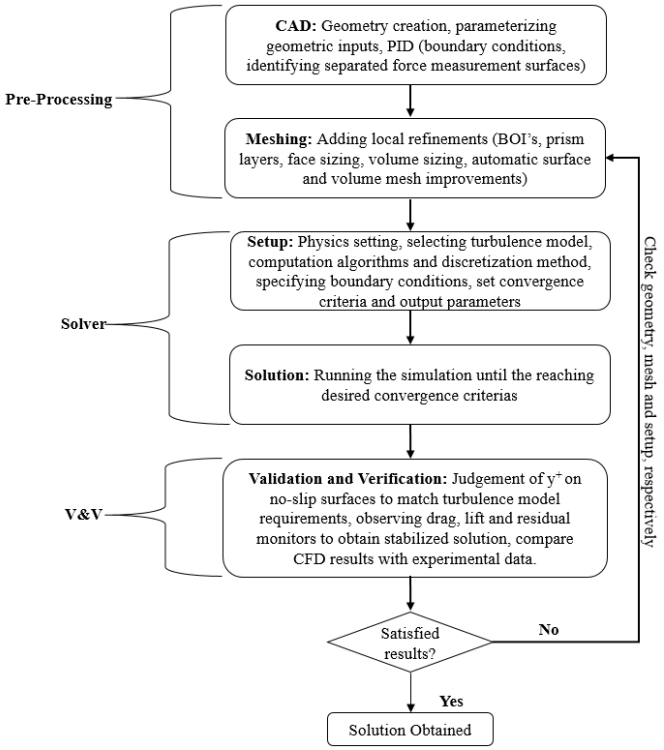

Figure 9. Procedures for CFD simulations

3. Finding and Discussions

3.1 Validation

Numerical analysis results in this study were compared in Table 4 including some numerical and experimental studies that existed in the literature. These reference studies both include numerical results (Thabet et al., 2018) and experimental results (Ahmed et al., 1984) (Meile et al., 2011). Reference studies selected considering similar boundary settings as possible with the current study however some there can be some differences in the sense of flow domain, turbulence model, Reynolds number, or total mesh number. One of the main experimental references was (Ahmed et al., 1984) made all tests with 60 m/s air stream. This corresponds to a Reynolds number of 4.29 million based on body length. This Reynolds number was approximately 2.1 million higher than the current study. The second experimental reference

study by (Meile et al., 2011) investigated the effect of slant angle using 25 ° and 35 °. Experiments were conducted at a velocity range 10 m/s ≤ U∞ ≤ 40 m/s to see the effect of the Reynolds number but main strategy for this study is applying a constant velocity of 40 m/s which corresponds to Re = $2{,}784x10^6$to avoid interpreting chaotic too much results. When compared with these two experimental studies, deviation values for C_d coefficients were 12.68% (Ahmed et al., 1984) and 6.59% (Meile et al., 2011). The main reason for the deviation is airstream velocity was higher in Ahmet et. al study (Ahmed et al., 1984).

The numerical study carried out by (Thabet et al., 2018) used a realizable k-ε model and adopted an Ahmed body with different slant angles. To evaluate the effect of different slant angles on Ahmed body, 10-40 ° slant angle models were analyzed. When comparing the result of the 35° slant angle model, drag coefficient value of this study only deviates by 0.16%. This variation can be acceptable, and the C_d results of this current study are in good agreement with previous experimental and numerical results.

3.2 Evaluation of force coefficients

Table 4. Numerical studies result in comparison with reference studies

Model	**Thabet et al., 2018**	**Emmanuel et al.,**	**Ahmed et al ., 1984**	**Meile et al., 2012**	**Base**	**10d1h**	**10d2h**	**10d3h**	**10d4h**	**10d5h**
C_D	0.2949	0.2895	0.258	0.276	0.2954	0.2914	0.2864	0.2863	0.2865	0.2878
C_L	0.0205	n.a	n.a	0.004	0.018	0.026	0.0685	0.0518	0.018	0.0546
Model	**15d1h**	**15d2h**	**15d3h**	**15d4h**	**15d5h**	**20d1h**	**20d2h**	**20d3h**	**20d4h**	**20d5h**
C_D	0.2862	0.2858	0.2856	0.2859	0.286	0.2855	0.2852	0.2851	0.2851	0.2854
C_L	0.062	0.064	0.0619	0.0501	0.096	0.0686	0.0547	0.0487	0.0359	0.017

The biggest drag reduction was attained by 3.5 % with 20D3H, while the lowest drag reduction was 2.5 % with 10D5H compared with to the base model which is 0.2945. It can be seen from Table 4, that increasing dimple diameter provides a positive effect on decreasing drag value, but the dimple depth factor causes a negative effect after a certain point. According to numerical results in Table 4, all dimple models enable a drag reduction when compared with the reference base Ahmed body model.

3.3. Comparison of wake flow structures

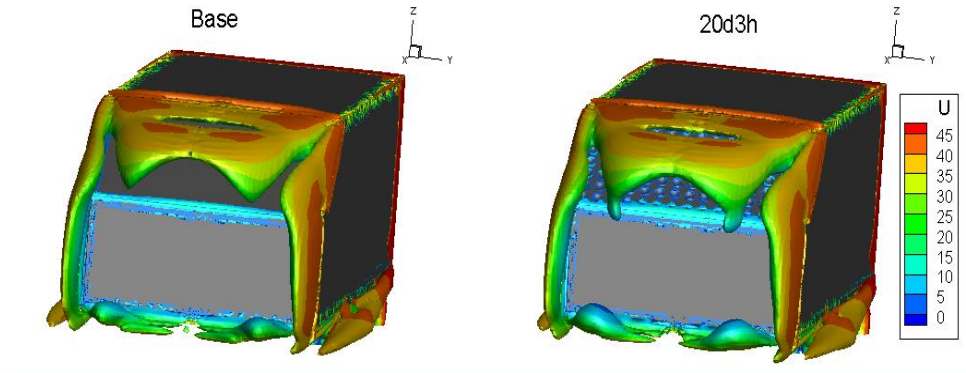

Figure 10. Iso-surfaces of Q criterion demonstration for numerical analysis

In this part of the study, qualitative flow representations were carried out between the optimum model with minimum drag (20d3h) and the base model. According to Figure 10, Q criterion can be seen, which was one of the vortex demonstration methods in fluid dynamics. The Q criterion defines vortices as 3D where the vorticity magnitude is greater than the magnitude of the rate of strain. For these two models, it is possible to see upper, lower, and longitudinal flow separation from the rear of the body. The obvious difference was lower and upper wakes tended to interact with each other more compared with the base model. This interaction resulted in a smaller wake region and provided pressure recovery at the rear of the body.

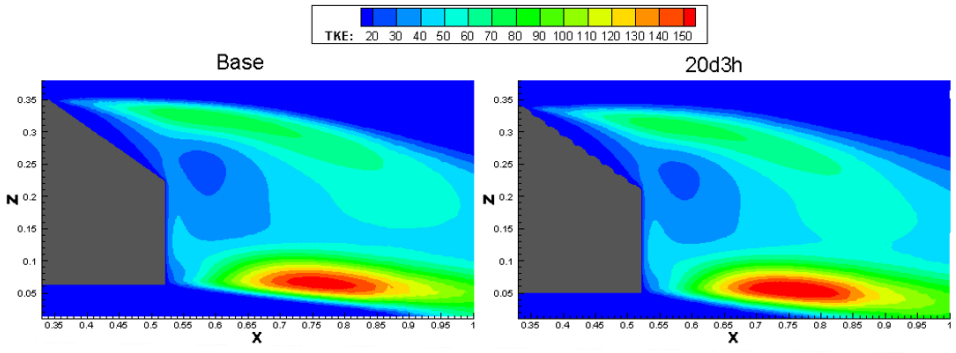

Figure 11. Turbulence kinetic energy (TKE (m^2/s^2)) contours in the symmetry plane

TKE is the qualitative measure of energy dissipation and loss for a given flow. It can be measured as the root mean square of the fluctuation in the flow velocity. TKE contours demonstrated higher energy loss due to higher drag. TKE contours in Figure 11 support previous comments about these two models. As can be seen, the lower and upper flow tended to interact at the rear of the body. The upwash and downwash break off clearly in the base model, but the same flows interact with each other in the 20d3h model. This indicated that the flow was is tending to a regular and uniform flow behavior.

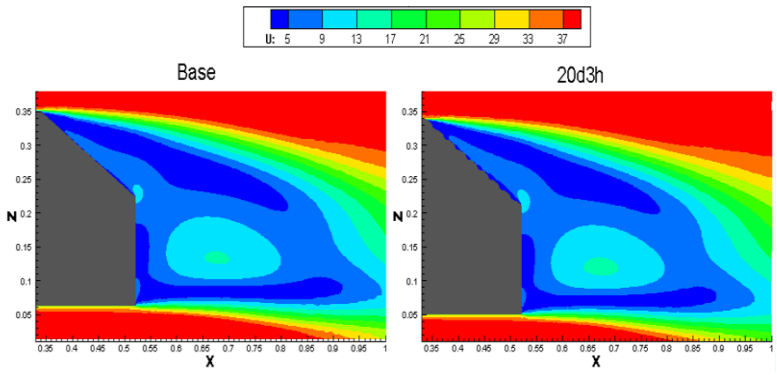

Figure 12. Velocity magnitude (u (m/s)) contours in the symmetry plane

A regular and narrower wake are essential in terms of aerodynamic performance for a vehicle. Ahmed body rear wake was almost independent of the front and longitudinal surfaces. That was why in this study drag reduction surfaces affected only the wake zone of the body. For the base model, it is possible

to see a bigger wake region on the rear however, optimized model using dimple surfaces enabled a smaller wake and provided pressure and velocity recovery. When comparing the end of the two contours it can be seen dark blue velocity regions were smaller and terminated before according to the base model. Also, the size of the green elliptical region in the middle of the contours is bigger than compared to the base model. When this information is evaluated, there was a velocity recovery using dimple surfaces.

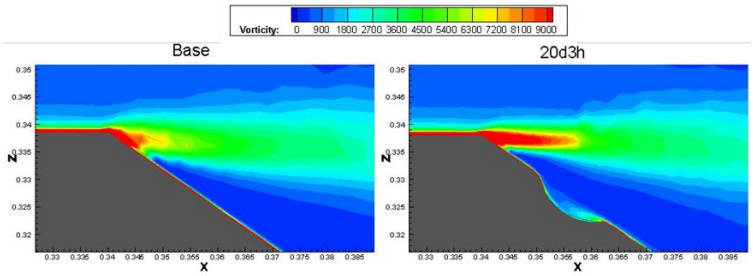

Figure 13. Vorticity (1/s) contours in the rear separation zone

Figure 13 shows vorticity magnitude contours in the symmetry plane. One of the main aims of using dimple surfaces was to eliminate or delay flow separation from the rear surface. The vorticity contours were represented in terms of the cohesion effect between flow particles and the vehicle surface. In Figure 13, since there was an elongation during the separation rear corner of the vehicle it can be said that an improvement has been gained in terms of attaching to the surface. According to the vorticity distribution of the rear area and it can be understood that dimple surfaces increased the power of the vortex by downwashing.

Table 5. Location of the planes

	Location		Location
X_1	x/L=0.1	Y_1	z/H=0.574
X_2	x/L=0.2	Y_2	z/H=1
X_3	x/L=0.3	Symmetry	y/W=0

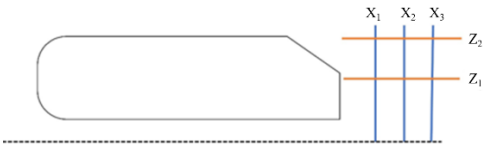

Figure 14. Demonstration of planes

In Figure 15 normalized velocity contours are demonstrated using X_1, X_2 and X_3 planes. These planes the vehicle from top to bottom also exact locations can be found in Figure 14 and Table 5. Naturally, as the distance increases from the vehicle surface, the size and value of velocity contours are reduced. But when evaluating the same distance level of planes, the optimized model's contours have smaller velocity regions according to base models. The more apparent difference can be seen for the upper velocity profiles which prove the effect of usage dimples on the rear surface.

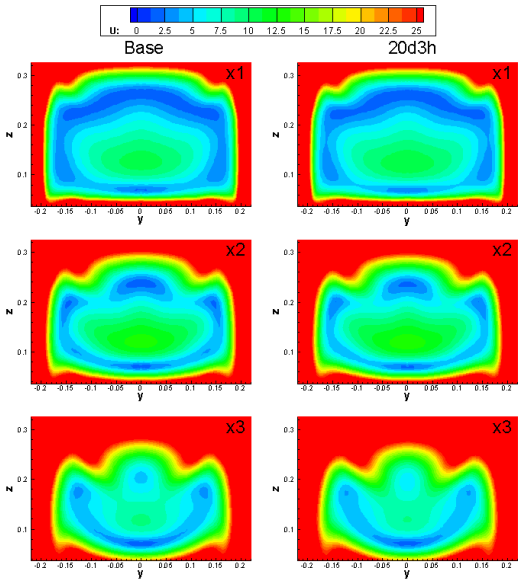

Figure 15. Velocity (m/s) magnitude contours with vertical planes ($\boldsymbol{X_1}$, $\boldsymbol{X_2}$, $\boldsymbol{X_3}$)

In Figure 16, velocity magnitude contours are illustrated with two horizontal planes. Z_2 plane locates upper side and Z_1 plane locates on the lower side of the vehicle. It can be seen from the contours at the $\boldsymbol{Z_2}$, the velocity values are smaller and create a flow separation for base model compared to the flow contour optimized model. However, with the optimized 20d3h model, the wake region is narrowing. Especially Z_2 contours show that there is a remarkable velocity recovery with the 20d3h model which can be attributed to drag reduction. Moreover, smaller wake is obvious for the optimized model compared with the base model at the $\boldsymbol{Z_2}$.

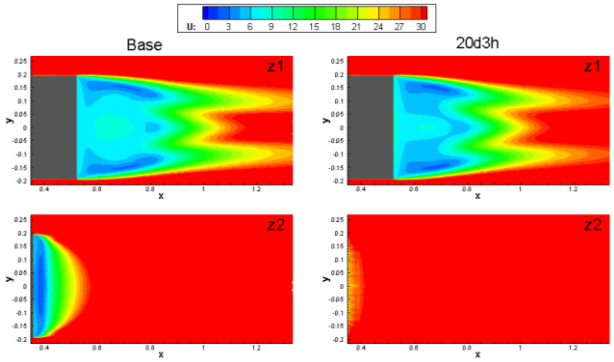

Figure 16. Velocity (m/s) magnitude contours with horizontal planes ($\boldsymbol{Z_1}$, $\boldsymbol{Z_2}$)

4. Conclusions

In this study, a drag reduction study was represented to improve the aerodynamic characteristics of a generic car model's rear wake zone. The dimpled rear window surface of Ahmed body with the 35° slant angle was optimized with variable parameters in each model. This study showed similar results to the main reference study by (Chear et al., 2015) in terms of passive drag reduction methods. These passive methods reduced pressure gradients by creating friction on the flow boundary layer. Inferences from this study can be summarized below:

- The dimpled surface could decrease the drag coefficient up to some certain design parameters.
- Although increasing dimple diameter affects positive, the higher dimple depth caused to increase in drag coefficient value after some certain point.
- Despite the optimized model reduces C_{D} value, there was no consistent variance on C_{L} values between optimized models and base models.

To conclude, it can be said that dimple surfaces reduce wake and turbulent intensity on the rear of the Ahmed's body. Especially flow separation zones are very critical to improving aerodynamic performance. In future studies, surface roughness techniques such as dimples, and vortex generators, can be applied to different zones of the car like bottom, top, side, and front surfaces, and their combinations. Moreover, considering that the drag reduction values are considerably low compared to vehicle size, it creates a discussion subject of whether this study is feasible or not. Also, it should be considered in terms of the commercial side because changing vehicle part shapes affects production conditions and it is important for the manufacturers whether it will be preferred visually or not.

Conflict of interest

The authors declare that there is no conflict of interest.

References

Abd-Alla GH. Using exhaust gas recirculation in internal combustion engines: a review. Energy Conversion and Management 2002; 43: 1027-1042.

Ahmed SR., Ramm G., Faltin G. Some salient features of the time-averaged ground vehicle wake. SAE Transactions 1984; 93(2): 473-503.

Altaf A., Omar AA., Asrar W. Review of passive drag reduction techniques for bluff road vehicles. IIUM Engineering Journal 2014; 15(1): 61-69.

Bayraktar I., Landman D., Baysal O. Experimental and computational investigation of Ahmed body for ground vehicle aerodynamics. Journal of Commercial Vehicles 2001; 110(2): 321-331.

Bing-xin W., Zhi-gang Y., Hui Z. Active flow control on the 25°Ahmed body using a new unsteady jet. International Journal of Heat and Fluid Flow 2019; 79: 108459.

Brady M., Browand F., Hammache M., Heineck JT., Leonard A., McCallen R., Ross J., Rutledge W., Salari K., Storms B. Progress in reducing aerodynamic drag for higher efficiency of heavy-duty trucks (Class 7-8). Lawrence Livermore National Laboratory Technical Report UCRL-JC-132873 1999; California, United States.

Chear CK., Dol SS. Vehicle aerodynamics: Drag reduction by surface dimples. International Journal of Mechanical and Mechatronics Engineering 2015; 9(1): 202 – 205.

Howell J., Sherwin C., Passmore M., Le Good G. Aerodynamic drag of a compact SUV as measured on-road and in the wind tunnel, SAE Technical Papers 2002; 2002-01-0529.

IMO. Third IMO GHG Study 2014 - Executive Summary and Final Report. 1 ed. International Maritime Organization 2015; London, UK, 1-327.

Jakirlic S., Jester-Zürker R., Tropea C. 9th Ercoftac/Iahr/Cost Workshop on Refined Turbulence Modelling 2001.

Kamal MNF., Ishak IA., Darlis N., Maji DSB., Sukiman SL., Rashid RA., Azizul MA. A review of aerodynamics influence on various car model geometry through CFD techniques. Journal of Advanced Research in Fluid Mechanics and Thermal Sciences 2021; 88(1): 109-125.

Kapadia S., Roy S., Wurtzler K. Detached eddy simulation over a reference Ahmed car model. in Direct and Large-Eddy Simulation Eds. Friedrich VR., Geurts BJ., Métais O. Springer, Dordrecht 2004.

Krajnović S., Davidson L. Large-eddy simulation of the flow around simplified car model, SAE Technical Papers 2004.

Leroyer A., Wackers J., Queutey P., Guilmineau E. Numerical strategies to speed up CFD computations with free surface-Application to the dynamic equilibrium of hulls. Ocean Engineering 2011; 38, 2070-2076.

Lienhart H., Stoots C., Becker S. Flow and turbulence structures in the wake of a simplified car model (Ahmed Model). New Results in Numerical and Experimental Fluid Mechanics III 2022; 77: 323-330.

McNally JW., Alvin FS., Mazellier N., Kourta A. Active flow control on an Ahmed body - An experimental study, in 53rd AIAA Aerospace Sciences Meeting 2015; 1-15.

Meile W., Brenn G., Reppenhagen A., Lechner B., Fuchs A. Experiments and numerical simulations on the aerodynamics of the Ahmed body. CFD Letters 2011; 3(1): 32-39.

Menter FR. Improved Two-Equation k-turbulence models for aerodynamic flows. NASA Technical Memorandum 1992; 103975.

Muyl F., Dumas L., Herbert V. Hybrid method for aerodynamic shape optimization in automotive industry. Computers and Fluids 2004; 33(5–6): 849–858.

Peter JEV., Dwight RP. Numerical sensitivity analysis for aerodynamic optimization: A survey of approaches. Computers and Fluids 2010; 39(3): 373–391.

Strachan RK., Knowles K., Lawson NJ. The vortex structure behind an Ahmed reference model in the presence of a moving ground plane. Experiment in Fluids 2007: 42(5): 659–669.

Thabet S., Thabit TH. CFD Simulation of the air flow around a car model (Ahmed Body). International Journal of Scientific and Research Publications 2018; 8(7): 517-525.

Vino G., Watkins S., Mousley P., Watmuff J., Prasad S. Flow structures in the near wake of the Ahmed model. Journal of Fluids and Structures 2005; 20(5): 673-695.

Yagiz B., Kandil O., Pehlivanoglu YV. Drag minimization using active and passive flow control techniques. Aerospace Science and Technology 2012; 17(1): 21–31.